ULTRAVIOLET SPECTROSCOPIC INVESTIGATION OF HU AQR AND AN UMa WITH THE DATA FROM HST AND IUE

M. R. Sanad

National Research Institute of Astronomy and Geophysics, Astronomy Department, Helwan – Cairo, Egypt; mrsanad1@yahoo.com

Received: 2015 July 27; accepted: 2015 August 31

We present ultraviolet spectroscopic study of two polar systems, HU Aqr and AN UMa, observed with the Hubble Space Telescope's Space Telescope Imaging Spectrograph (STIS) and Faint Object Spectrograph (FOS) and with the International Ultraviolet Explorer (IUE) during the period 1979–2003, to diagnose the ultraviolet fluxes of C IV 1550 Å and He II 1640 Å emission lines originating in an accretion stream during different orbital phases. The reddening of two systems is determined from the 2200 Å absorption feature. Different spectra for both systems, showing the variations in line fluxes at different orbital phases, are presented. We concentrated on calculating the line fluxes of CIV and He II emission lines. From HST and IUE data, we derived accretion luminosities and accretion rates for the two systems. The average temperature of the accretion stream for HU Aqr and AN UMa is about 5000 K and 6000 K, respectively. Our results show that there are variations in line fluxes, accretion luminosities and accretion rates with time for the two systems. These modulations are attributed to the variations of both density and temperature as a result of a changing rate of mass transfer from the secondary star to the primary star. These results from the HST and IUE observations support the irradiation model producing sufficient ultraviolet flux for orbital modulations.

Key words: accretion – stars: individual (HU Aqr, AN UMa) – cataclysmic variables – ultraviolet: stars

1. INTRODUCTION

Polars, or AM Herculis type stars, are interacting binary objects. The primary is a white dwarf with a magnetic field of the order of a few tens of MG. The secondary is a lower main-sequence red dwarf which fills its Roche Lobe. It loses gas at the inner Lagrangian point and this gas falls towards the primary in a stream.

The gas in the stream is ionized by collisions and X-rays from the accretion region surrounding the primary, so at some point in the stream's trajectory the magnetic energy density of the primary's field is sufficient to divert the stream from its free fall trajectory and force it to follow the field lines.

Accretion, therefore, occurs over a small area near one or both magnetic poles of the white dwarf. Material in the stream is traveling at roughly the escape velocity of the white dwarf when it approaches the surface of the white dwarf, so a strong shock forms in the accretion flow close to the surface. Being interacting

red dwarf – white dwarf pairs, polars are a class of cataclysmic variables (CVs). For a review of cataclysmic variables and polars, see (Cropper 1990; Warner 1995; Wu 2000; Beuermann 2002; Wu et al. 2003).

HU Aqr is a magnetic cataclysmic variable of the AM Herculis type. It was detected in the ROSAT-XRT and ROSAT-WFC all sky surveys (Hakala et al. 1993; Schwope et al. 1993), where its binary nature and the eclipse were discovered. HU Aqr has an orbital period of 2.08 h, and the white dwarf's magnetic field strength is estimated to be 37 MG, (Schwope et al. 1993; Glenn et al. 1994). HU Aqr consists of a 0.8 M_{\odot} white dwarf that accretes material from a 0.18 M_{\odot} main-sequence companion star (Schwope et al. 2001).

Previous observations of HU Aqr have been obtained in all wavelengths from X-rays to IR (Schwope et al. 1997, 2001, 2003, 2011; Schwarz et al. 2009; Watson et al. 2003; Howell et al. 2002; Bridge et al. 2002; Harrop-Allin et al. 1999, 2001; Vrielmann & Schwope 2001; Heerlein et al. 1999; Glenn et al. 1994).

AN UMa is also a magnetic cataclysmic variable of the AM Herculis type. It was discovered by (Krzeminski & Serkowski 1977) and identified as the second after AM Herculis polar due to its high polarization. AN UMa has an orbital period of 1.91 h, and the white dwarf magnetic field strength is estimated to be 35.8 MG, (Cropper et al. 1989). AN UMa contains a low-mass white dwarf ($M_{\rm wd} = 0.4$ –0.6 M_{\odot}) with a temperature of $\approx 20\,000$ K (Bonnet-Bidaud et al. 1996).

Previous photometric and spectroscopic observations of AN UMa have been reported in a number of papers (Campbell et al. 2008; Kafka & Honeycutt 2005; Ramsey et al. 2004; Bonnet-Bidaud et al. 1996; Ramseyer et al. 1993; Imamura et al 1986; Szkody et al. 1981, 1988).

Here we present an analysis of the Hubble Space Telescope (HST) and International Ultraviolet Explorer (IUE) observations of HU Aqr and AN UMa. In Section 2 we describe the UV spectroscopy and data analysis techniques. In Section 3 we briefly discuss the determination of the reddening of each of the systems. In Section 4 we discuss the results of the analysis and its implications concerning the spectral behavior of both HU Aqr and AN UMa, as well as the reasons behind the observed variability. Comparison between the spectral behavior of HU Aqr and AN UMa is presented in Section 5. Finally, concluding remarks are presented in Section 6.

2. OBSERVATIONAL DATA AND REDUCTIONS

2.1. IUE SWP low-resolution spectra of HU Aqr and AN UMa

The IUE low-resolution short wavelength spectra have been retrieved from the INES (IUE Newly Extracted Spectra) system through its principle center¹. A full description of the INES system for low-resolution data is given by Rodriguez-Pascual et al. (1999) and Gonzalez et al. (2001).

The observational data were processed using the standard ESO MIDAS package for the processing of spectra. We referenced the spectra to the orbital phase of the HU Aqr system using the ephemeris of Schwope et al. (1997),

 $HJD = 2448896.543707(27) + 0.086820446(9) \times E$

http://ines.vilspa.esa.es

Table 1. Journal of IUE observations of HU Aqr.

Image ID	Dispersion	Aperture	J.D.	Exposure time (s)	Phase
SWP52187	Low	Large	2449619.1	2400	0.46
SWP52188	Low	Large	2449619.2	6420	0.45
SWP52189	Low	Large	2449619.3	7860	0.77
SWP55043	Low	Large	2449887.4	9480	0.23

Table 2. Journal of IUE observations of AN UMa.

Image ID	Dispersion	Aperture	J.D.	Exposure time (s)	Phase
SWP07052	Low	Large	2444178.4	18000	0.15
SWP07053	Low	Large	2444178.6	7200	0.99
SWP29548	Low	Large	2446732.2	22200	0.63
SWP29552	Low	Large	2446733.2	5580	0.65
SWP30311	Low	Large	2446841.1	15600	0.44
SWP47008	Low	Large	2449039.0	7200	0.32

Table 3. Journal of HST observations of HU Aqr.

Data set	Instrument	Aperture	Grating	J.D.	Exposure time (s)	Phase
Y3F3A103T	FOS	1.0-PAIR	G160L	2450325.8	235.898	0.16
Y3F3A104T	FOS	1.0-PAIR	G160L	2450325.9	2582.969	0.74
Y3F3A105T	FOS	1.0-PAIR	G160L	2450326.0	2582.969	0.51
Y3F3A106T	FOS	1.0-PAIR	G160L	2450326.1	2582.969	0.28
Y3F3A107T	FOS	1.0-PAIR	G160L	2450326.1	2582.969	0.06
Y3F3A108T	FOS	1.0-PAIR	G160L	2450326.2	2582.969	0.83
Y3F3A201T	FOS	1.0-PAIR	G160L	2450338.8	1408.242	0.78

Table 4. Journal of HST observations of AN UMa.

Data set	Instrument	Aperture	Grating	J.D.	Exposure time (s)	Phase
O6LI45010	STIS	52X0.2	G140L	2452814.04	900	0.28

and for the AN UMa system using the ephemeris of Imamura et al. (1986),

 $HJD = 2443190.9921(\pm 0.0002) + 0.07975320(\pm 0.00000003) \times E.$

Tables 1 and 2 list the IUE observations for HU Aqr and AN UMa with low resolution. The spectra were inspected individually in the 1150-1950 Å region to identify and reject noisy and overexposed or underexposed data.

We present available observations of IUE for HU Aqr and AN UMa covering most of their orbital phases. Representative examples of emission lines are given in Figs. 1, 2 and 3, showing the variations of line fluxes at different times. These lines are produced in an accretion stream for the two systems.

2.2. HST spectra of HU Agr and AN UMa

The HST Space Telescope Imaging Spectrograph (STIS) and Faint Object Spectrograph Far Ultraviolet (FOS FUV) spectra of HU Aqr and AN UMa have been retrieved from the HST archive system². For a full description of STIS and

 $^{^2}$ http://archive.stsci.edu

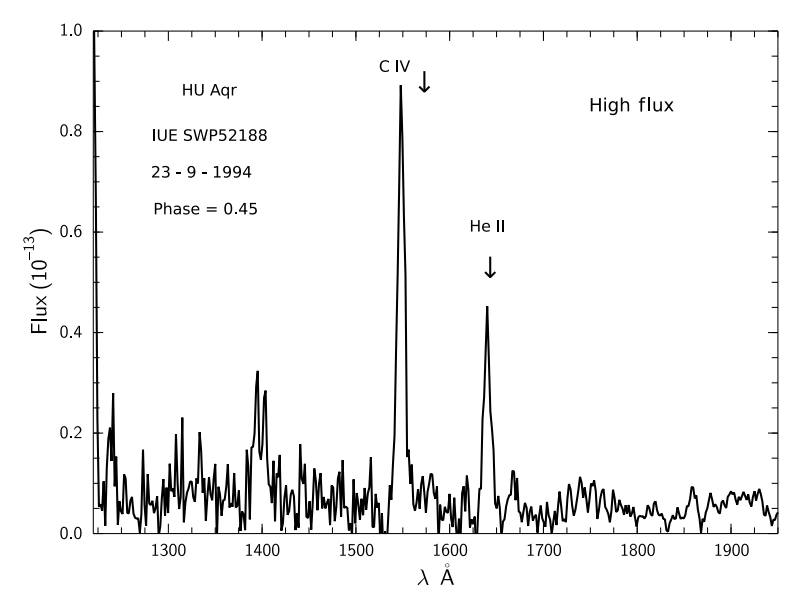


Fig. 1. IUE spectrum of HU Aqr with high flux at phase 0.45. The flux is plotted in units of $\rm erg\,cm^{-2}\,s^{-1}\,\AA^{-1}$.

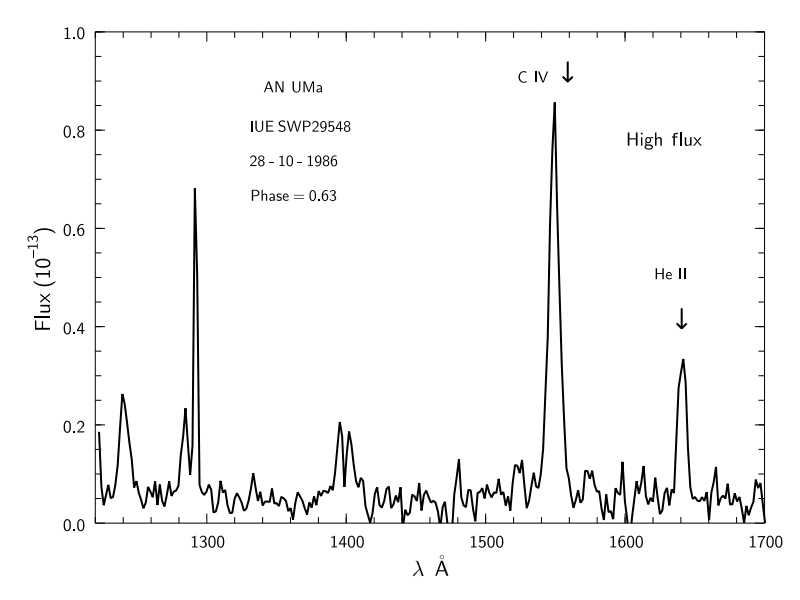


Fig. 2. IUE spectrum of AN UMa with high flux at phase 0.63. The flux is plotted in units of ${\rm erg\,cm^{-2}\,s^{-1}\,\mathring{A}^{-1}}$.

FOS, see Kimble et al. (1998), Woodgate et al. (1998) and Harms & Fitch (1991). The retrieved data were processed using the standard ESO MIDAS package for the processing of spectra. We analyzed the HST/FOS spectra of HU Aqr using the G160L grating and 1.0 aperture, and the HST/STIS spectra for AN UMa using

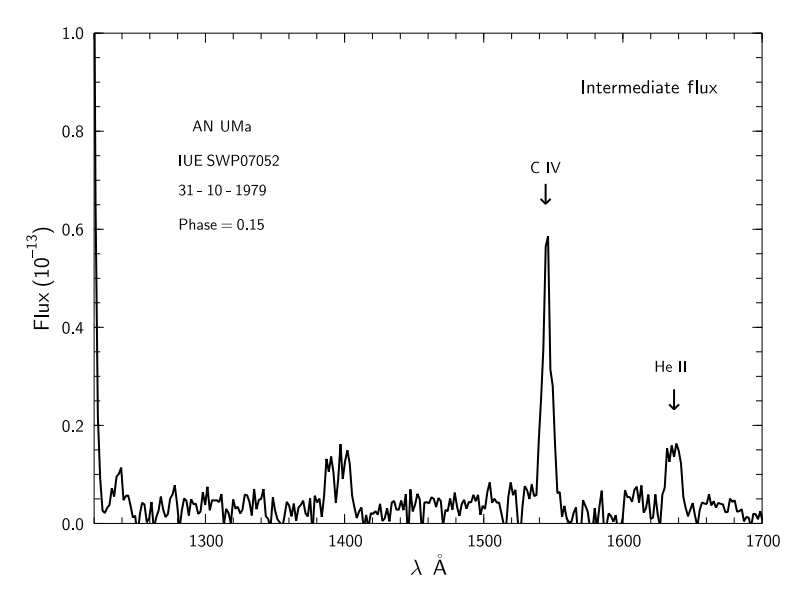


Fig. 3. IUE spectrum of AN UMa with intermediate flux at phase 0.15. The flux is plotted in units of ${\rm erg\,cm^{-2}\,s^{-1}\,\AA^{-1}}$.

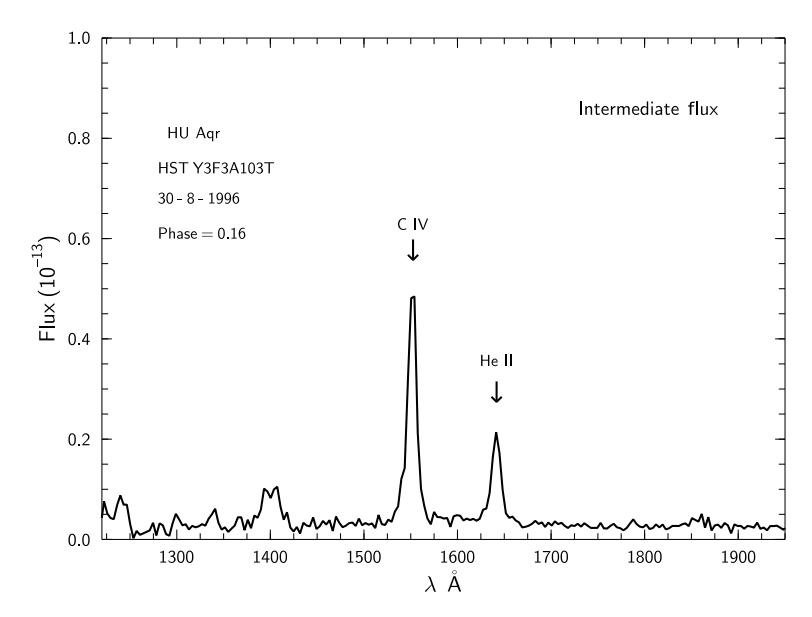


Fig. 4. IUE spectrum of HU Aqr with intermediate flux at phase 0.16. The flux is plotted in units of $\rm erg\,cm^{-2}\,s^{-1}\,\AA^{-1}$.

the G140L grating and 52×0.2 aperture. The details of these observations are listed in Tables 3 and 4. Representative examples of emission lines are given in Figs. 4, 5 and 6, showing the variations in line fluxes at different times. For both star systems these lines are produced in the accretion streams.

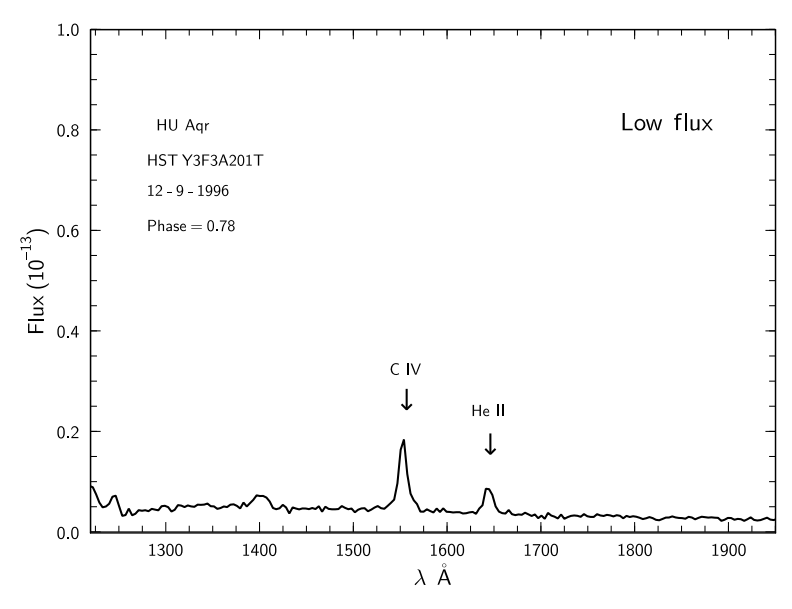


Fig. 5. IUE Spectrum of HU Aqr with low flux at phase 0.78. The flux is plotted in units of $\rm erg\,cm^{-2}\,s^{-1}\,\mathring{A}^{-1}$.

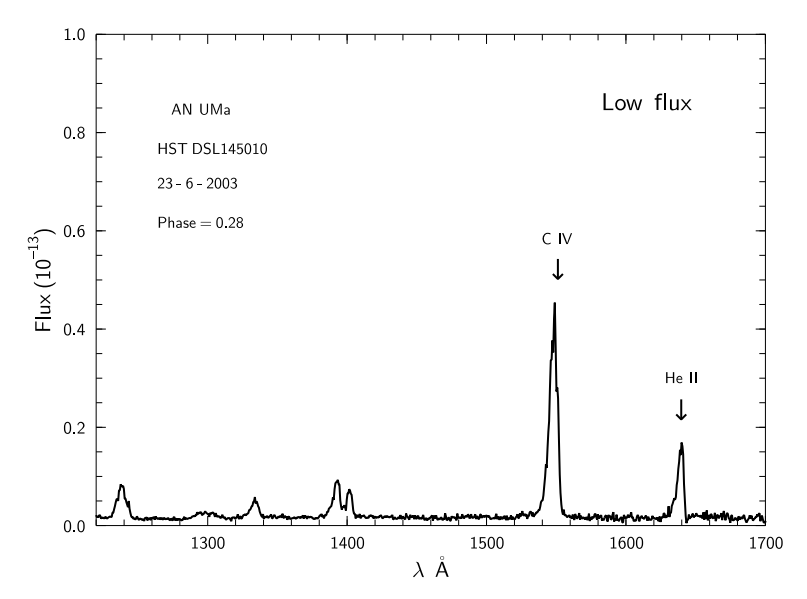


Fig. 6. IUE Spectrum of AN UMa with low flux at phase 0.28. The flux is plotted in units of $\operatorname{erg\,cm^{-2}\,s^{-1}\,\mathring{A}^{-1}}$.

3. REDDENING DETERMINATIONS

The reddening of HU Aqr and AN UMa can be estimated from the 2200 Å absorption feature. We determined the reddening with the best set of short wavelength and long wavelength spectra. We binned the flux measurements into 15 Å

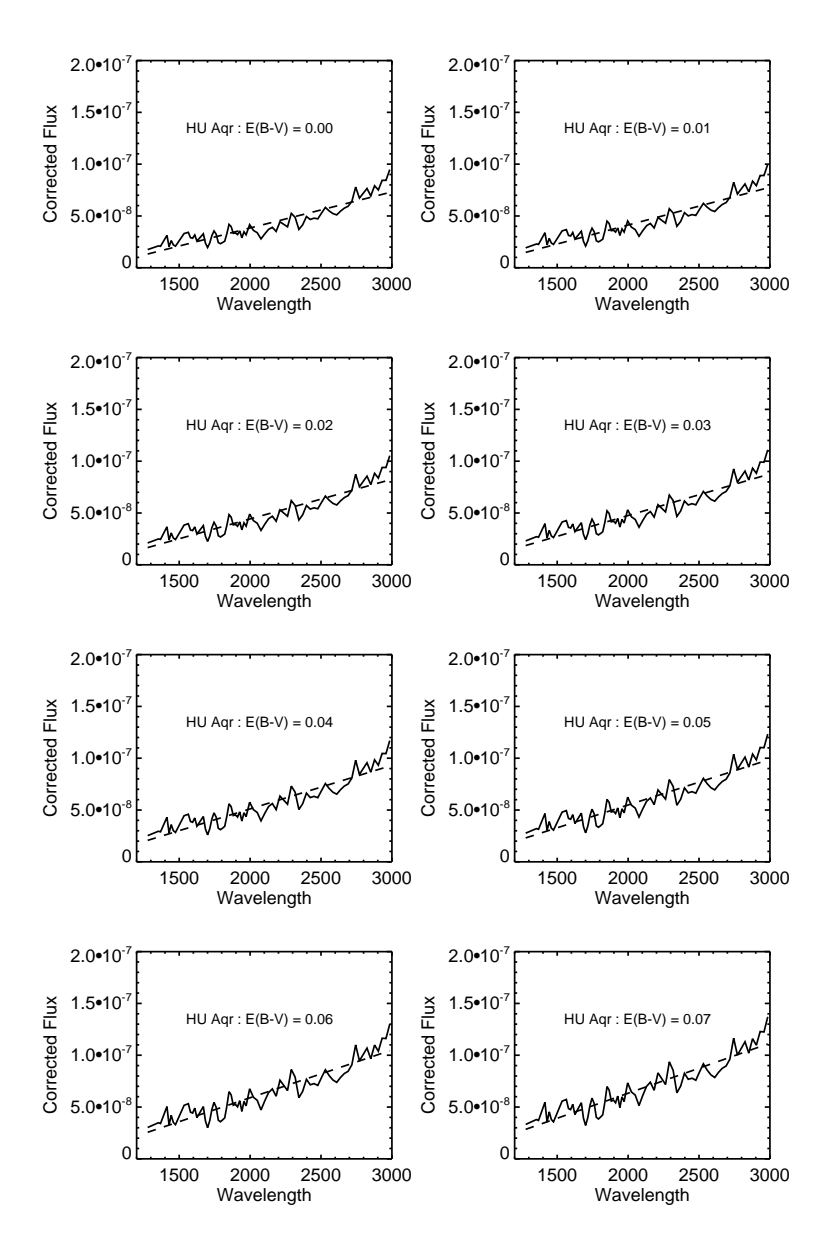


Fig. 7. Reddening determination for HU Aqr.

intervals for short wavelength and 25 Å intervals for long wavelength. The acceptable range of values for E_{B-V} is found by visual inspection of the plots for the best fit for 2200 Å. We estimated E_{B-V} for both HU Aqr and AN UMa to be 0.00 mag, as illustrated in Figs. 7 and 8.

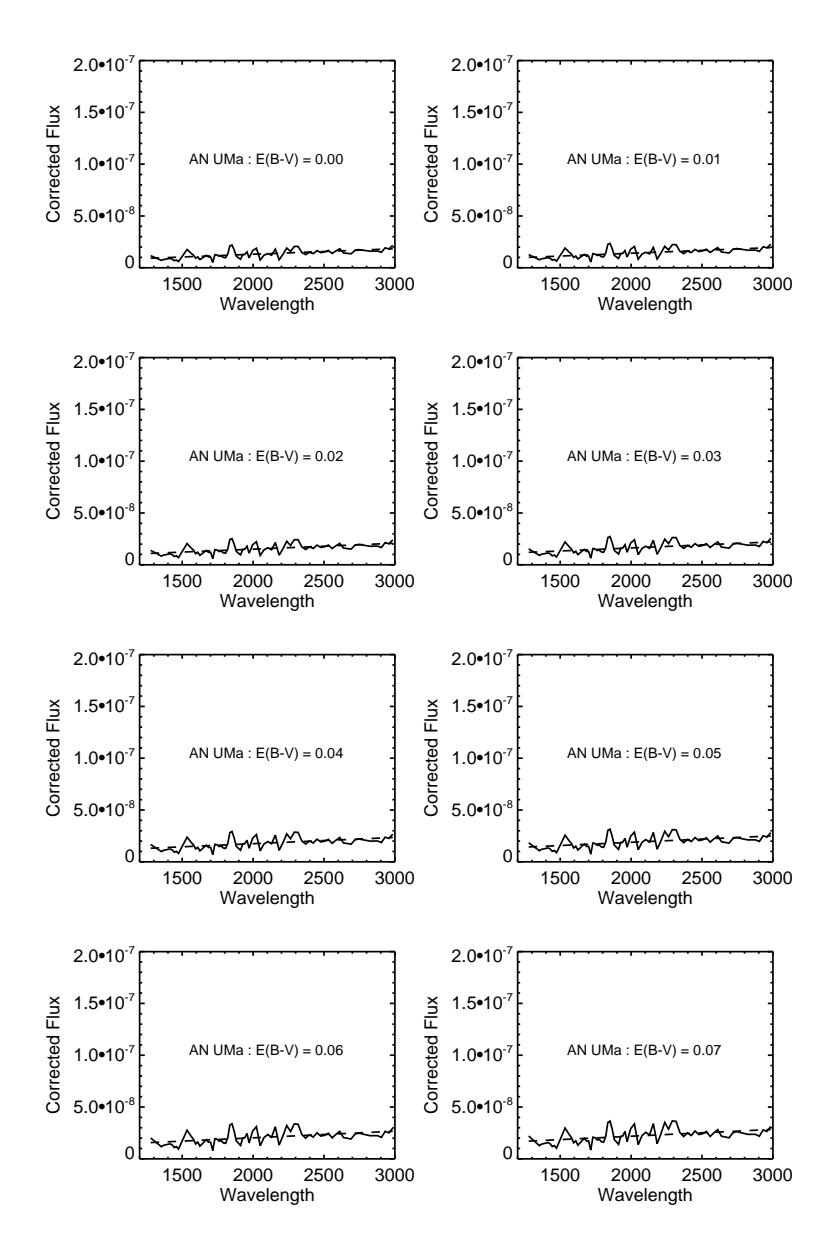


Fig. 8. Reddening determination for AN UMa.

4. RESULTS AND DISCUSSION

4.1. Method for calculating the fluxes of emission lines

We fit the observed portions of the emission line wings with a Gaussian function. The "integrate/line" command in the ESO/MIDAS suite was interactively used to determine the continuum level and to integrate the flux of the C IV 1550 Å

and He II 1640 Å emission lines above this continuum. For the calculations of line fluxes, we calculated the integrated fluxes for the emission lines in $\operatorname{erg cm}^{-2} \operatorname{s}^{-1}$.

4.2. Behavior of the emission lines in HU Agr and AN UMa

The CIV emission line at 1550 \mathring{A} is a resonance spectral line, while He II emission line at 1640 \mathring{A} is a recombination line. Figs. 9, 10, 11 and 12 show the behavior of line fluxes with orbital phase for the CIV and He II emission lines. The line fluxes vary with orbital phase between high, intermediate and low values on a short time scale of hours and days, and on a long time scale of years. Line fluxes of CIV vary by a factor of six, while the line fluxes of He II vary by a factor of two. The line fluxes of CIV and He II for HU Aqr increase smoothly to a maximum value at orbital phase around 0.5 and then decrease to a minimum value at orbital phase around 0.8. The line fluxes of CIV and He II for AN UMa increase smoothly to a maximum value at orbital phase around 0.6 and then decrease to a minimum value at orbital phase around 0.95.

The HST and IUE observations presented here can be understood in the framework of the following physical interpretations. Let us suppose that the ultraviolet emission lines originate from optically thin region in the accretion stream. The high energy photons created in the accretion stream do indeed produce the ultraviolet emission lines observed in HU Aqr and AN UMa.

Physically, the total luminosity of HU Aqr and AN UMa is related to its mass transfer rate. An increase in mass transfer leads to an increase in the rate of gravitational potential energy release, and, consequently, an increase in the intensity of ultraviolet emission lines produced by the accretion stream.

The variations of line fluxes are attributable to variations in mass accretion rate, variations in accretion geometry, progressive eclipsing of the accretion stream, variations in density, and variations in temperature.

The irradiation model provides a good description of the present HST and IUE data. In this model the accretion stream is strongly affected by irradiation coming from the white dwarf, leading to variations in line fluxes.

During the high fluxes when mass accretion is strong, the ultraviolet spectrum is dominated by strong emission lines, clearly indicating their connection to the increased mass accretion. During the low fluxes when mass accretion is weak or stopped, most of the emission lines are absent or are very weak. During an intermediate mass accretion, emission lines with intermediate fluxes do appear.

For HU Aqr, by using integrated fluxes of C IV 1550 Å and He II 1640 Å and adopting a mean value of 134 pc for the star's distance derived by Ciardi et al. (1998), we find from the equation

$$L_{\rm UV} = 2\pi F d^2 \tag{1}$$

that ultraviolet luminosities for the two spectral lines are variable. For different flux values (high, intermediate and low) the observed luminosities are the following:

The ultraviolet luminosities for HU Aqr are greater than those of the EU UMa polar system, and comparable to the ultraviolet luminosities of the ST LMi polar system, see Sanad (2015).

For a white dwarf of mass $M \approx 0.8 M_{\odot}$ and a radius of 7×10^8 cm (Schwope et al. 1997) the mass accretion rates are calculated from the equation

$$\dot{M} = L_{\rm UV} R_{\rm a} / G M_{\rm a},\tag{2}$$

where $M_{\rm a}$ and $R_{\rm a}$ are the mass and radius of the accreting star, $L_{\rm UV}$ is the accretion luminosity, and G is the gravitational constant. Based on high, intermediate and low flux values the accretion rates for HU Aqr are the following:

$$\begin{array}{lll} \mbox{High flux} & \dot{M}_{\rm C\,IV} \approx 2 \times 10^{13} \ \mbox{g\,s}^{-1} \ (3.17 \times 10^{-13} \ M_{\odot} \ \mbox{yr}^{-1}), \\ \mbox{Intermediate flux} & \dot{M}_{\rm C\,IV} \approx 7 \times 10^{12} \ \mbox{g\,s}^{-1} \ (1.11 \times 10^{-13} \ M_{\odot} \ \mbox{yr}^{-1}), \\ \mbox{Low flux} & \dot{M}_{\rm C\,IV} \approx 3 \times 10^{12} \ \mbox{g\,s}^{-1} \ (4.76 \times 10^{-14} \ M_{\odot} \ \mbox{yr}^{-1}); \\ \mbox{High flux} & \dot{M}_{\rm He\,II} \approx 5 \times 10^{12} \ \mbox{g\,s}^{-1} \ (7.93 \times 10^{-14} \ M_{\odot} \ \mbox{yr}^{-1}), \\ \mbox{Intermediate flux} & \dot{M}_{\rm He\,II} \sim 2 \times 10^{12} \ \mbox{g\,s}^{-1} \ (3.17 \times 10^{-14} \ M_{\odot} \ \mbox{yr}^{-1}), \\ \mbox{Low flux} & \dot{M}_{\rm He\,II} \sim 9 \times 10^{11} \ \mbox{g\,s}^{-1} \ (1.42 \times 10^{-14} \ M_{\odot} \ \mbox{yr}^{-1}). \end{array}$$

These results are comparable with those from Schwope et al. (2003). The accretion rates for HU Aqr are greater than those of the EU UMa polar system, and comparable to the accretion rates of the ST LMi polar system, see Sanad (2015).

To determine the temperature of the accretion stream for high, intermediate and low states, the Stefan-Boltzmann equation

$$L = \sigma A T^4 \tag{3}$$

is used. Here, the Stefan-Boltzmann constant σ is $\sim 5.6704 \times 10^{-5}$ erg cm⁻² s⁻¹ K⁻⁴, and A is the surface area. We consider the accretion stream geometry as a thin cone (Howell et al. 1999). We deal with the area of the base, which is a circle, πr^2 , and the outer radius set to be 3.16×10^9 cm (Cropper 1990). The temperature of the accretion stream for HU Aqr, based on the high flux values, low flux values, and intermediate flux values, is ~ 6000 K, ~ 5000 K, and ~ 4000 K, respectively.

For AN UMa, by using integrated fluxes of C IV 1550 Å and He II 1640 Å and adopting a mean value of 330 pc for the distance derived by Schmidt et al. (1986), we find variable ultraviolet luminosities for the two spectral lines:

$$\begin{array}{lll} \mbox{High flux} & L_{\rm C\,IV} \approx 5 \times 10^{30} \ \mbox{erg s}^{-1} & L_{\rm He\,II} \approx 2 \times 10^{30} \ \mbox{erg s}^{-1}, \\ \mbox{Intermediate flux} & L_{\rm C\,IV} \approx 4 \times 10^{30} \ \mbox{erg s}^{-1} & L_{\rm He\,II} \approx 9 \times 10^{29} \ \mbox{erg s}^{-1}, \\ \mbox{Low flux} & L_{\rm C\,IV} \approx 2 \times 10^{30} \ \mbox{erg s}^{-1} & L_{\rm He\,II} \approx 4 \times 10^{29} \ \mbox{erg s}^{-1}. \end{array}$$

The ultraviolet luminosities for AN UMa are greater than those of the EU UMa polar system, and comparable to the ultraviolet luminosities of the ST LMi polar system (Sanad 2015).

For a white dwarf of mass $M \approx 0.4 M_{\odot}$, a radius of 1.082×10^9 cm is calculated by using the equation

$$R_{\rm WD} = 0.78 \times 10^9 \left[\left(\frac{1.44 M_{\odot}}{M_{\rm WD}} \right)^{2/3} - \left(\frac{M_{\rm WD}}{1.44 M_{\odot}} \right)^{2/3} \right]^{1/2}.$$
 (4)

The accretion rates for AN UMa are the following:

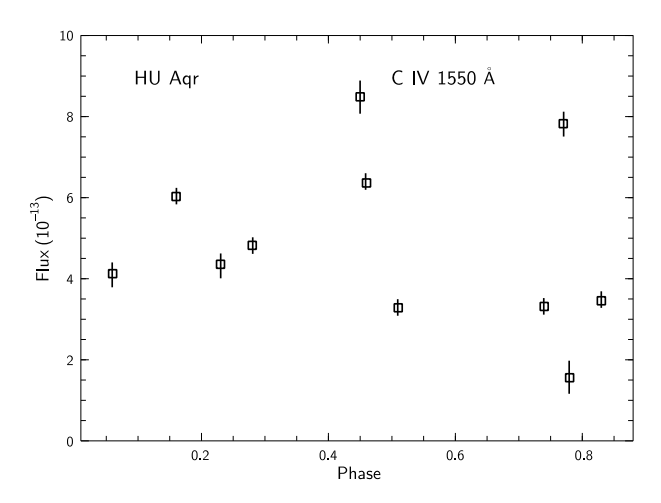


Fig. 9. Variation of the CIV line flux with phase for HU Aqr. The 1σ error bars are shown on each data point. The flux is plotted in units of erg cm⁻² s⁻¹.

$$\begin{array}{lll} \mbox{High flux} & \dot{M}_{\rm C\,IV} \sim 1 \times 10^{14} \ \mbox{g\,s}^{-1} \ (1.59 \times 10^{-12} \ M_{\odot} \ \mbox{yr}^{-1}), \\ \mbox{Intermediate flux} & \dot{M}_{\rm C\,IV} \sim 7 \times 10^{13} \ \mbox{g\,s}^{-1} \ (1.11 \times 10^{-12} \ M_{\odot} \ \mbox{yr}^{-1}), \\ \mbox{Low flux} & \dot{M}_{\rm C\,IV} \sim 4 \times 10^{13} \ \mbox{g\,s}^{-1} \ (6.34 \times 10^{-13} \ M_{\odot} \ \mbox{yr}^{-1}); \\ \mbox{High flux} & \dot{M}_{\rm He\,II} \sim 4 \times 10^{13} \ \mbox{g\,s}^{-1} \ (6.34 \times 10^{-13} \ M_{\odot} \mbox{,yr}^{-1}), \\ \mbox{Intermediate flux} & \dot{M}_{\rm He\,II} \sim 2 \times 10^{13} \ \mbox{g\,s}^{-1} \ (3.17 \times 10^{-13} \ M_{\odot} \mbox{yr}^{-1}), \\ \mbox{Low flux} & \dot{M}_{\rm He\,II} \sim 9 \times 10^{12} \ \mbox{g\,s}^{-1} \ (1.42 \times 10^{-13} \ M_{\odot} \mbox{yr}^{-1}). \end{array}$$

These results are comparable with those of Schwope et al. (2003). The accretion rates for AN UMa are greater than those of the EU UMa polar system and comparable to the accretion rates of the ST LMi polar system, see Sanad (2015).

The temperature of the accretion stream for AN UMa, based on the high flux values, low flux values, and intermediate flux values is $\sim\!7000$ K, $\sim\!6500$ K, and $\sim\!5500$ K, respectively.

The variations of line fluxes between high, intermediate and low values stem from the variations of both density and temperature as a result of changing rate of mass transfer from the secondary star to the white dwarf are similar to that found for other polar systems – V834 Cen and MR Ser (see Sanad 2012). The line flux variability of the CIV and He II emission lines seem to be more compatible with the irradiation model producing sufficient ultraviolet flux for orbital modulations. Tables 5, 6, 7 and 8 show the fluxes of the CIV and He II emission lines. The errors for the measured line fluxes are in the range of 1σ . The uncertainty in the values of line fluxes was determined using the procedures outlined by Lenz & Ayers (1992) and Bruhweiler (2002).

5. COMPARISON BETWEEN THE SPECTRAL BEHAVIOR OF HU Aqr AND AN UMa IN ULTRAVIOLET

Figs. 1, 4, 5, 9 and 10, which display the line fluxes of HU Aqr as a function of orbital phase for the C IV and He II emission lines, along with the corresponding Figs. 2, 3, 6, 11 and 12 for AN UMa, reveal the following results.

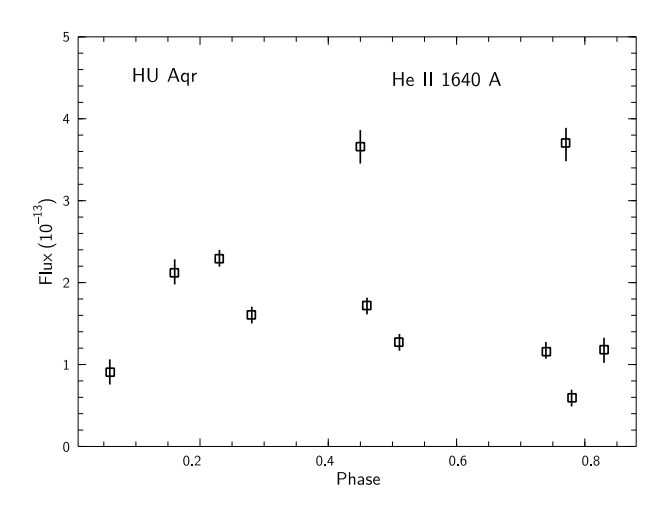


Fig. 10. The same as in Figure 9, but for the He II line.

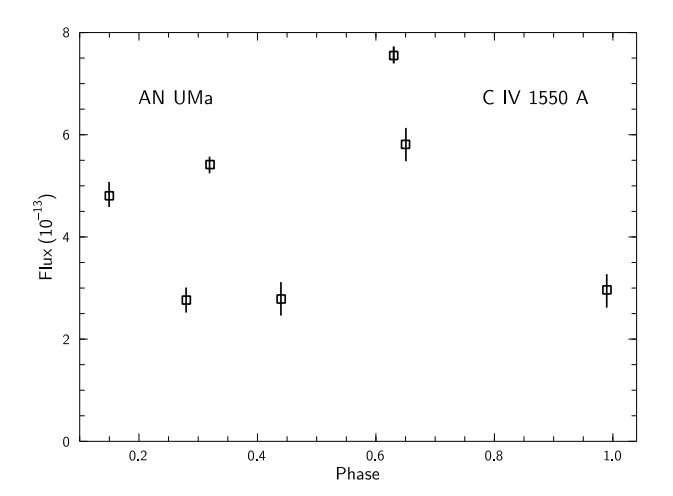


Fig. 11. Variation of the C IV line flux with phase for AN UMa. The 1σ error bars are shown on each data point. The flux is plotted in units of erg cm⁻² s⁻¹.

Table 5. Line fluxes of HU Aqr from the IUE spectra. The integrated fluxes are in units of 10^{-13} erg cm⁻² s⁻¹.

Image ID	J.D.	Line flux CIV	Line flux He II	Phase
SWP52187	2449619.1	6.36	1.72	0.46
SWP52188	2449619.2	8.48	3.65	0.45
SWP52189	2449619.3	7.82	3.70	0.77
SWP55043	2449887.4	4.35	2.29	0.23

- 1. The ultraviolet continuum for HU Aqr is approximately the same as that for AN UMa.
- 2. The flux values of C IV 1550 Å and He II 1640 Å for HU Aqr are comparable with those for AN UMa, indicating that the characteristics of the primary com-

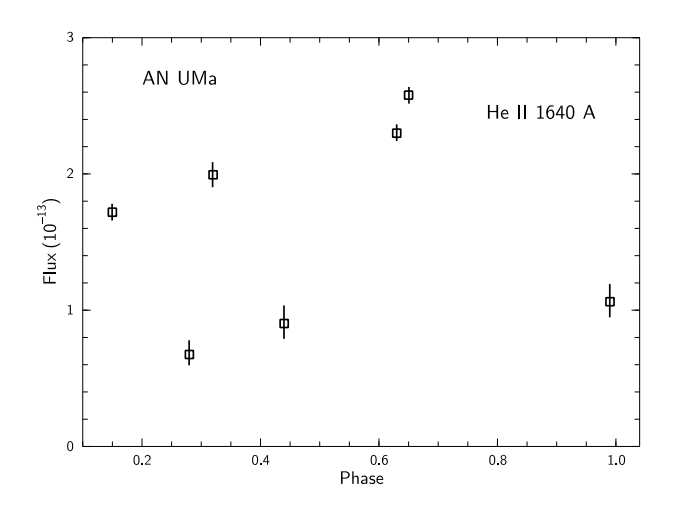


Fig. 12. The same as in Figure 11 but for the He II line.

Table 6. Line fluxes of HU Aqr from the HST spectra. The integrated fluxes are in units of 10^{-13} erg cm⁻² s⁻¹.

Data set	J.D.	Line flux CIV	Line flux He II	Phase
Y3F3A103T	2450325.8	6.02	2.12	0.16
Y3F3A104T	2450325.9	3.31	1.15	0.74
Y3F3A105T	2450326.0	3.28	1.27	0.51
Y3F3A106T	2450326.1	4.82	1.60	0.28
Y3F3A107T	2450326.1	4.12	0.90	0.06
Y3F3A108T	2450326.2	3.45	1.18	0.83
Y3F3A201T	2450338.8	1.55	0.59	0.78

Table 7. Line fluxes of AN UMa from the IUE spectra. (The integrated fluxes are units of 10^{-13} erg cm⁻² s⁻¹.

Image ID	J.D.	Line flux C IV	Line flux He II	Phase
SWP07052	2444178.4	4.81	1.72	0.15
SWP07053	2444178.6	2.96	1.06	0.99
SWP29548	2446732.2	7.55	2.30	0.63
SWP29552	2446733.2	5.81	2.38	0.65
SWP30311	2446841.1	2.79	0.90	0.44
SWP47008	2449039.0	5.42	1.99	0.32

Table 8. Line fluxes of AN UMa from the HST spectra. The integrated fluxes are in units of 10^{-13} erg cm⁻² s⁻¹.

Data set	J.D.	Line flux CIV	Line flux ${\rm HeII}$	Phase
O6LI45010	2452814.04	2.76	0.67	0.28

ponents (which determine, to a large extent, the physics involved in the accretion process) are similar, producing similarities in the form and intensity of the emitted spectrum.

3. The ultraviolet luminosity and accretion rate of HU Aqr are approximately

comparable with those of AN UMa.

4. The average temperature of the accretion stream for HU Aqr and AN UMa is ~ 5000 K and ~ 6000 K, respectively.

6. CONCLUSIONS

In this paper we presented ultraviolet spectroscopic study of the two polar systems, HU Aqr and AN UMa, based on the IUE and HST observational data. We concentrated on studying two emission lines, CIV 1550 Å and He II 1640 Å, for both systems. We confirmed the presence of variations in line flux, ultraviolet luminosity and accretion rate for both systems.

We attributed the modulations of line fluxes, ultraviolet luminosities and accretion rates to the changes of both density and temperature as a result of a changing rate of mass transfer from the secondary star to the primary star.

The analysis is based on the assumption that the ultraviolet radiation is coming from one pole. The temperature of accretion stream is calculated by using the Stefan-Boltzmann equation. The variations of ultraviolet spectral line fluxes with orbital phases for HU Aqr and AN UMa can be explained by the irradiation model producing sufficient ultraviolet fluxes for orbital modulations.

REFERENCES

Beuermann K. 2002, PASP, 114, 472

Bonnet-Bidaud J. M., Mouchet M., Somova T. A., Somov N. N. 1996, A&A, 306, 199

Bridge C. M., Cropper M., Ramsay G. et al. 2002, MNRAS, 336, 1129

Bruhweiler F. 2002, private communication

Campbell R. K., Harrison T. E., Mason E. et al. 2008, ApJ, 678, 1304

Ciardi D. R., Howell S. B., Dhillon V. S. et al. 1998, PASP, 110, 1007

Cropper M. 1990, SSRv, 54, 195

Cropper M., Mason K. O., Allington-Smith J. R. et al. 1989, MNRAS, 236, 29

Glenn J., Howell S. B., Schmidt G. D. et al. 1994, ApJ, 424, 967

González-Riestra R., Cassatella A., Wamsteker W. 2001, A&A, 373, 730

Hakala P. J., Watson M. G., Vilhu O. et al. 1993, MNRAS, 263, 61

Harms R., Fitch J. 1991, SPIE, 1494, 49

Harrop-Allin M. K., Cropper M., Hakala P. J. et al. 1999, MNRAS, 308, 807

Harrop-Allin M. K., Potter S. B., Cropper M. 2001, MNRAS, 326, 788

Heerlein C., Horne K., Schwope A. D. 1999, MNRAS, 304, 145

Howell S. B., Cash J., Mason K. O., Herzog A. E. 1999, AJ, 117, 1014

Howell S. B., Ciardi D. R., Sirk M. M., Schwope A. D. 2002, AJ, 123, 420

Imamura J. N., Steiman-Cameron T. Y. 1986, ApJ, 311, 786

Kafka S., Honeycutt R. K. 2005, AJ, 130, 742

Kimble R. A., Woodgate B. E., Bowers C. W. et al. 1998, ApJ, 492, L83

Krzeminski W., Serkowski K. 1977, ApJ, 216, L45

Lenz D. D., Ayers T. R. 1992, PASP, 104, 1104

Ramsay G., Cropper M., Wu K. et al. 2004, MNRAS, 350, 1373

Ramseyer T. F., Robinson E. L., Zhang E. et al. 1993, MNRAS, 260, 209

Rodríguez-Pascual P. M., González-Riestra R., Schartel N., Wamsteker, W. 1999, A&AS, 139, 183

Sanad M. R. 2012, IJAA, 2, 218

Sanad M. R. 2015, NewA, 36, 110

Schmidt G. D., Stockman H. S., Grandi S. A. 1986, ApJ, 300, 804

Schwarz R., Schwope A. D., Vogel J. et al. 2009, A&A, 496, 833

Schwope A. D., Mantel K., Horne K. 1997, A&A, 319, 894

Schwope A. D., Schwarz R., Sirk M., Howell S. B. 2001, A&A, 375, 419

Schwope A. D., Thomas H. C., Beuermann K. 1993, A&A, 271, L25

Schwope A. D., Thomas H. C., Mantel K. et al. 2003, A&A, 402, 201

Schwope A. D., Horne K., Steeghs D., Still, M. 2011, A&A, 531A, 34

Szkody P., Schmidt E., Crosa L., Schommer R. 1981, ApJ, 246, 223

Szkody P., Mateo M. Downes R. 1988, PASP, 100, 362

Vrielmann S., Schwope A. D. 2001, MNRAS, 322, 269

Warner B. 1995, Cataclysmic Variable Stars, Cambridge Univ. Press, Cambridge

Watson C. A., Dhillon V. S., Rutten R. G. M., Schwope A. D. 2003, MNRAS, 341, 129

Woodgate B. E., Kimble R. A., Bowers C. W. et al. 1998, PASP, 110, 1183

Wu K. 2000, Sp. Sci. Rev., 93, 611

Wu K., Cropper M., Ramsay G. et al. 2003, Chin. J. Astron. Astrophys., 3 (Suppl.), 235